



# High-Speed, High-Accuracy Core Point Detection Method for Fingerprint Recognition Systems

*Mr.Y.Praveen Konda Reddy<sup>1</sup>., Narsapuram Lavanya<sup>2</sup>*

*1 Assistant Professor, Department of CSE, Malla Reddy College of Engineering for Women.,  
Maisammaguda., Medchal., TS, India*

*2, B.Tech CSE (21RG5A0515),*

*Malla Reddy College of Engineering for Women., Maisammaguda., Medchal., TS, India*

## Abstract

*Fingerprint identification systems employ the central point to speed up the alignment process between fingerprints. It is more practical to develop image processing algorithms utilizing integrated modules to speed up processing for real-time applications. Suitable for usage in transportable computing devices. This may be achieved if the algorithm has a straightforward structure that makes it practical for use on embedded modules. This research proposes a mask that can identify the center of the image just by consulting the ridge orientation map. The described approach can identify the central point at the conclusion of a broken line in a grayscale orientation map. The singular areas are shown to be situated at the terminus of this discontinuous line, which is shown by use of a mathematical property.*

## 1. Introduction

Today, biometric authentication systems based on fingerprints are commonplace. Many consumer electronics include them, including computers and mobile phones. Most embedded systems rely on inexpensive digital modules like field-programmable gate arrays. [1, 2] or DSP [3]. Many international airports now utilize fingerprint authentication methods. In addition, forensics relies heavily on them to identify hidden evidence at crime scenes. Most of these uses are real-time systems that can't afford to wait more than a few seconds for the authentication process to complete. Alignment between the two compared fingerprints makes use of global characteristics including singular points (SPs), the core, and the delta points [4-6]. Core point (CP), which is specified for all fingerprint kinds, is a more dependable point. The standard method is a comparison of both fingerprints without any alignment in between. However, with this alignment, the detailed feature set for each fingerprint is aligned relative to the CP, drastically cutting down on computing time [7].

Ridges are the line patterns that make up the fingerprint. The parallel ridges go along smoothly. The singular regions (SRs) of these surfaces are much curved [8]. As can be seen in Fig. 1, both a loop and a delta form fall under this category. The loop is the most inwardly recurring ridge; it must circle back Along its original path. As may be seen in Fig. 2, it has two distinct manifestations. Up is indicated by the convexity of the top loop. On the upper loop, we establish a core point at the top. In most fingerprints, it may be seen in the middle [9]. That Convex Lower Loop component is angled downwards. Only when an upper loop is present does it exist. In the delta area, the ridges' flow splits into two branches [4, 10]. According to Fig. 1, a delta point is located at the intersection of the three ridge flow directions [5]. The noun for the uppermost core point is "core point." (CP). In the published works, the CP is defined in many ways. The highest point of the innermost ridge line is its definition [8]. In some other advanced



*Figure 1 A fingerprint image with a loop and a delta region.*



*Figure 2 shows the fingerprint's upper and lower loop shapes.*

Work, it is defined as the location along the fingerprint ridges where the curvature is greatest [11, 12]. Henry forensics and definition these specifications are similar to those in [14], however the CP is defined as the point farthest from the delta point on the shoulder of the loop. The points that are manually retrieved are always ridge-based definitions. According to the existence of the SPs, the fingerprint pictures are divided into five distinct categories [8]. One core and one delta point are found in each of the two loops, left and right.

Two cores and two delta points characterize the whorl shape. There are three distinct varieties of arch. One core and one delta points make up the tented arch. There is no loop in the up-thrust arch, although the ridges do undergo a somewhat abrupt transition. There are no SPs in the simple arch. The CP is one of the SPs that can be detected using a variety of methods [8], some of which are based on the Poincare Index (PI) [15], others on the local characteristics of the ridge orientation [16,17], still others on finding the point of intersection between partitions of the ridge orientation [11], and still others on detecting both the orientation map and the SPs simultaneously using a mathematical model like the 2D Fourier Expansion (2D FOMFE) [18]. The PI technique [8] is the traditional method of SP detection. It is the total amount of rotation that occurs within a closed circle. Depending on this total value, the presence of an SP and its kind is determined. Its merits are: the simplicity of design, resilience to the picture rotation and the determination of the singularity type [19]. It's susceptible to background noise, however. The symmetries of a tensor orientation field with complex values may be found with the use of techniques that employ complex filters [17].



However, their CP detection in the arch type fingerprint has limited accuracy. The semi-radial symmetry filter, which is more powerful but more complicated, has recently been introduced. Then, using an orientation variation based feature [20], we can get rid of the outliers. Recently developed classes of CP detection techniques are described in [12, 21-23]. Grayscale ranging from 0 degrees to 180 degrees depicting the line seen on the ridge orientation map is used for this classification. The gap between the zero and 180 degrees creates this line. Using the edge detection approach [12, 21], a method based on an edge map may identify the DL and then pinpoint the CP by examining the orientation consistency at the DL's ends. Fast CP detection is possible using the edge map-based technique. The CP with the greatest amount of curvature along the DL is the target of a different technique [22]. This new class is related to partitioning-based approaches [11]. The SPs may be found by first partitioning the orientation map into a finite number of levels and then studying the places where these partitions overlap. Blocks make up the fingerprint picture. The fingerprint blocks are segmented using intensity mean and variance thresholding followed by morphological procedures. An adaptive smoothing approach [9] is utilized once the ridge orientation map has been measured using the gradient-based method [8]. After that, the CP mask is put on. When many points are found, the one with the lowest error is selected using orientation consistency in orientation smoothing. Consistent worth. The DL node with the lowest consistency value is selected if no point is found. To determine the CP orientation, researchers follow the steps outlined in [9]. The mask is evaluated on the following databases: FVC2002 DB1 and DB2 set (A) [25]; FVC2004 DB1 set (B) [26]. The suggested mask has a higher core detection rate and shorter detection time compared to the edge-map based technique. Here's how the remainder of the paper is laid out: In Section 2, we detail the progress made in detecting singularities. The orientation map is dissected in Section 3. The suggested method for locating the core is laid forth in Section 4. In Section 5 we provide and analyze the experimental findings. Section 6 provides the final analysis.

## 2. Developed aspect for singular point detection

After a generalization of a property concerning SP detection, a new property is introduced to confirm the SR's presence at the DL's conclusion. When the orientation map is quantized into a number of levels, the fault lines that result are lines where the SPs are located [11]. As can be seen in Fig. 3, the fault lines mark the boundaries of the similar areas. This attribute is described as:

When a directional picture is quantized into three directions, only the singular points are affected by the fault lines, which is Property 1. In [11], it is shown that the junction points lose clarity and sharpness as the number of quantized orientation levels (N) grows.

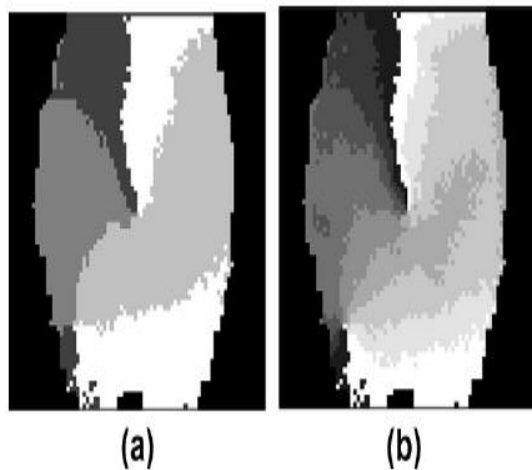




Figure 3 shows a 4-level and 9-level quantized orientation map.

The bare minimum required to unlock the SPs is level three. (N= 3). Given that fingerprint ridges lack any discernible direction, we may define orientation values as being inside the interval ((0\_ 6 h 180\_) and create a new condition that generalizes condition 1 as follows:

The second property states that "when an orientation map is quantized into a number of levels greater than two (N> 2)," the fault lines cross in the unique area. Proof. The evidence is developed independently for each SR type as follows: The orientation map identifies the core area as the innermost loop's "head" [22]. The points (x, y) on the innermost loop's curve have an orientation of u, therefore let's use that. (X, y). The set of orientation values on a loop may be expressed as follows, provided that a loop is a continuous ridge that recurs back to its initial direction [14].

$$\varphi(x_c, y_c) = \{(\theta_L + 0^\circ) \dots (\theta_L + 180^\circ)\} \quad (1)$$

Where the major direction of the loop's orientation, HL, is measured in degrees. Therefore, all possible orientations are scanned by the values at the innermost loop's curved portion. Consequently, the intersection of the fault lines produced by quantizing the orientation map into N=1 levels occurs in the central area.

The delta area originates from a third-flow direction created when two parallel ridges separate from one another. The set of (x, y) orientation values in the delta area may be expressed as follows, providing that the ridges flow has a constant slope.

$$\varphi(X_D, Y_D) = \{ \{ \varphi_i \dots (\varphi_i + a) \} \cup \{ (\varphi_i + a) \dots (\varphi_i + a + b) \} \cup \{ (\varphi_i + a + b) \dots \varphi_i \} \} \quad (2)$$

Where (u<sub>i</sub>) is the initial orientation of the two parallel ridges, (a) is the orientation value at the point where the first parallel ridge is parallel to the third direction, and (b) is the orientation value at the point where the two ridges diverge. And the orientation value b 2 0\_ ; 180\_ is found at the intersection of the second parallel ridge with the other half of the third direction. Therefore, all possible orientations are covered by the values in the delta area. As a result, the delta area will serve as a point of intersection for the fault lines that emerge as a result of quantizing the orientation map into an unlimited number of levels (N= 1). The SP is housed inside the SR. As can be seen in Fig. 3, the fault lines converge at a single point for N=4 quantization, but for N=9 quantization, the issue of out of focus arises due to the limitation of the orientation measurement. However, it is confined to a single area. Similarly, the SP may be found at the extremities of the DL that is created from orientation mapping [12, 21, and 23]. The DLs are not the same as the fault lines. The fault lines are the lines produced by quantizing the orientation map into a number of levels; if there are two levels, the fault line is a continuous line without an end within the fingerprint region; if there are three levels, the fault lines meet at the SPs in three different places. However, the DLs always terminate at the SPs (in both the x and y directions) since they are created from the discontinuity of the orientation values between 0\_ and 180\_.

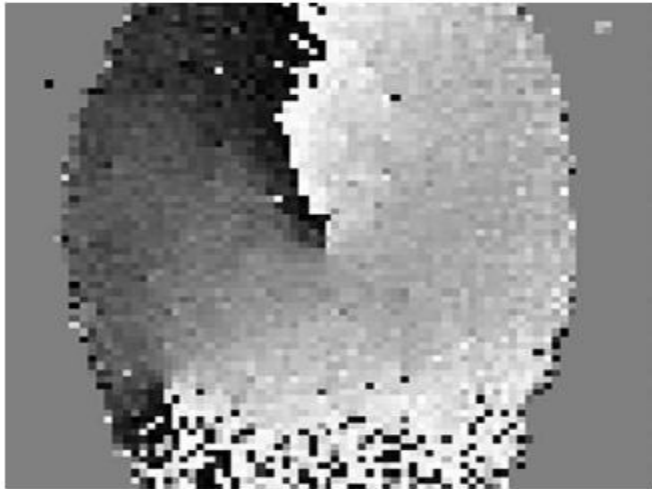


Figure 4: The original orientation map, before smoothing. However, there is no theoretical basis shown for this speculation.

The following brand-new development is intended to help with this shortage: Presented and established as Follows thirdly, if the endpoints of the discontinuous lines in the fingerprint's orientation map are not on the fingerprint's border, then the fingerprint's single area will be there. Proof. Two areas define the line produced by the break in the orientation map at the 0\_ and 180\_ positions:

$$R_a : \theta_a(X_a, Y_a) \text{ where } (0^\circ \leq \theta_a(X_a, Y_a) \leq a^\circ) \quad (3)$$

$$R_b : \theta_b(X_b, Y_b) \text{ where } (b^\circ \leq \theta_b(X_b, Y_b) < 180^\circ) \quad (4)$$

On one side of the DL is the area Ra with orientation values ha(x, y), on the other side of the DL is the region Rb with orientation values hb(x, y), and a b. This is the last sentence be in a third geographical area as determined by the RC of orientation values,

$$R_c : \theta_c(X_c, Y_c) \text{ where } (a^\circ < \theta_c(X_c, Y_c) < b^\circ) \quad (5)$$

Three areas ((3)-(5)) are found in the SR, derived from the core region (1) and the delta region (2) of Eq. As a result, the SR resides at the terminus of the DL. The end of the DL and the core point, or delta point, is shown in Fig. 4.

### 3. Orientation map analysis

Point (x, y) is the center of a tiny neighborhood, and the local ridge orientation is the direction of the ridges (or ridges and valleys [4]) relative to the horizontal. Axis. Each fingerprint pixel may have its orientation determined (h(x, y)), yielding what is known as a high resolution map of orientation [4]. There will be some overlapping of the neighborhoods. Block-wise calculation of orientation saves on processing time by dividing the picture into sections of size w • w, where w is somewhat larger than the ridge width. Each block's average orientation ho(i, j) is then



determined. Gradient-based methods are the standard for calculating orientation maps [8]. The equation for it is as follows:

$$\theta_o(i, j) = \frac{\pi}{2} + \frac{1}{2} \arctan \left[ \frac{2 \cdot G_{xy}}{G_{xx} - G_{yy}} \right] \quad (6)$$

$$G_{xx}(x, y) = \sum_{h=-b}^b \sum_{k=-b}^b \nabla_x(x+hy+k)^2 \quad (7)$$

$$G_{yy}(x, y) = \sum_{h=-b}^b \sum_{k=-b}^b \nabla_y(x+hy+k)^2 \quad (8)$$

$$G_{xy}(x, y) = \sum_{h=-b}^b \sum_{k=-b}^b \nabla_x(x+hy+k) \cdot \nabla_y(x+hy+k) \quad (9)$$

Where  $x$  and  $y$  are the pixel coordinates of the block's center point  $(i, j)$ ,  $\$$  is the basic Sobel filter [27], and  $b = (w/2\_1)$ . In order to get the mean on a normal distribution,  $w$  must be an odd number. Spread out on the plane. To counteract this tendency in discrete computing, using a window size that is an odd integer is recommended [6]. Grayscale representation of the ridge orientation map is shown in Fig. 4. The x-axis of the orientation values points to the right, while the y-axis points upwards; this is the standard axis. As can be seen in Fig. 5, it is also represented as a series of thin lines on the fingerprint picture. To improve the precision of the orientation map and, by extension, the precision of the CP detection, we use an adaptive smoothing approach [9] based on the orientation consistency. The precision of the CP position is preserved while the orientation map is smoothed out. How closely the ridge orientations in a neighborhood align with the dominant orientation is described by the term "orientation consistency." The SP may be found at the neighborhood



Figure 5 A magnified view of Fig. 1 that emphasizes the locations of the singularities.



The minimal consistent orientation. In [9], we get the smoothed orientation map by:

$$\theta_s(i, j) = \frac{1}{2} \arctan \left( \frac{\sum_{(k,l) \in \Omega(s)} \sin(2\theta_o(k, l))}{\sum_{(k,l) \in \Omega(s)} \cos(2\theta_o(k, l))} \right) \quad (10)$$

Where  $X(s)$  is the block's neighborhood, defined by the  $(2s + 1) \cdot (2s + 1)$  outer surrounding blocks, and  $h_s(i, j)$  is the smoothed orientation of the block  $(i, j)$ , where  $s$  denotes the degree of uniformity. This leads to the equation for orientation consistency:

$$cons(i, j, s) = \frac{\sqrt{\left( \sum_{(k,l) \in \Omega(s)} \cos(2\theta_o(i, j)) \right)^2 + \left( \sum_{(k,l) \in \Omega(s)} \sin(2\theta_o(i, j)) \right)^2}}{M} \quad (11)$$

In this case,  $M$  represents the total number of adjacent buildings. Figure 6 displays the refined orientation map. Figure 7 shows a three-dimensional representation of the orientation map after smoothing. The start corresponds to the top left corner of Fig. 6, and the z-axis shows the degrees of rotation. A white circle defines the CP. The ramp is round in design. Figure 8 displays the orientation values along the top DL of a high-resolution version of Figure 6. From the highest point to the center of the plot, the samples are laid out. The average value of the right side of the upper DL is close to  $180^\circ$ , as indicated in the figure. A median value close to  $0^\circ$  may be seen on the line's left side. As one approaches the CP, there is a convergence in the orientation values of the DL's sides. The convergence point is the intersection of the two loop axes, when the orientation values cancel out. In Figure 8, the CP is located at sample number 143. This is the region where the orientation value rises from its minimum around  $0^\circ$  values to its maximum at  $90^\circ$ . Back on the other side of the DL, the orientation values continue to rise as one curve counterclockwise.

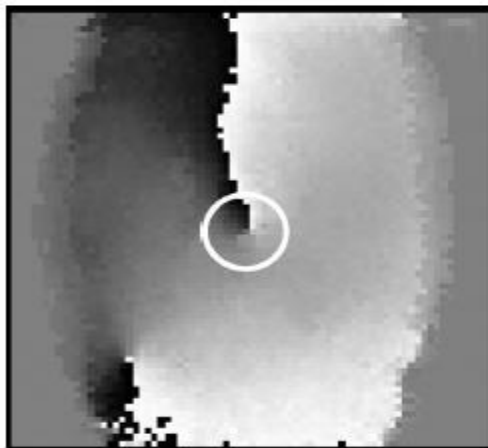
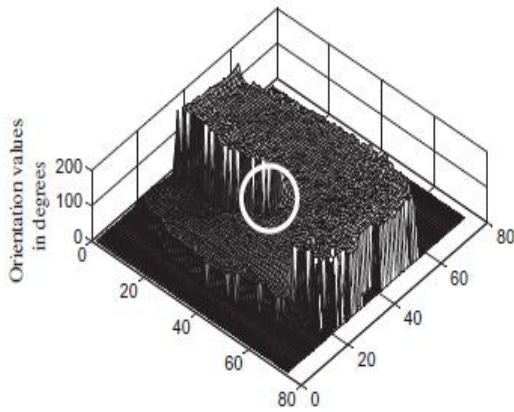




**Figure 6 Smoothed orientation map. The CP is circled.**



Orientation 3D graph shown in Figure 7. The fingerprint image's dimensions are the x and y coordinates.

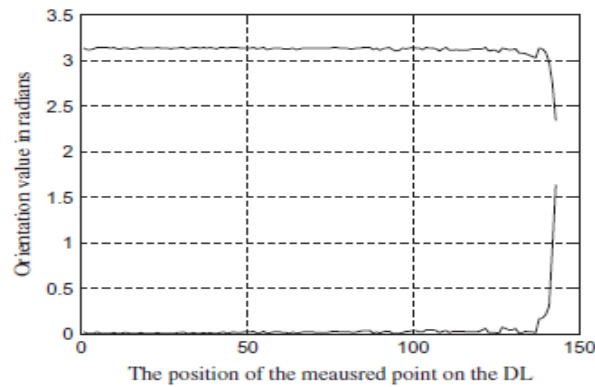


**Figure 8 the orientation values along a discontinuous line.**

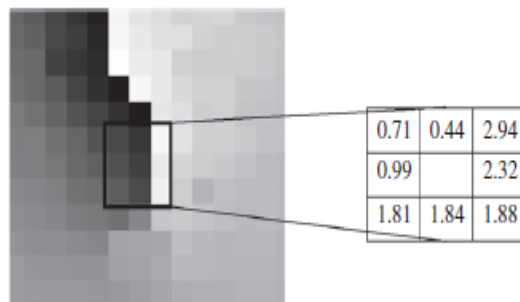


**Figure 9: Orientation map displaying CP orientation values (in radians).**

This investigation and the study performed on the orientation field of a zero-pole model [15] are both compatible with the CP. Figure 9 displays the values of block orientations relative to the CP. The value of the upper-middle



block is close to zero, whereas that of the upper-right block is close to one hundred eighty. Similar to the region of the loop when the sides are parallel, the values in the three bottom blocks are close together. In the blocks around the CP, the orientation values rise from close to 0 to close to 180 in a circular manner. Each and every CP manually retrieved from pictures 10 in the training set conforms to this orientation pattern. Above the CP, the orientation values shown in Fig. 10a are either high (160\_ 6 ho 180\_) or low (0\_ 6 ho 50\_). The orientation values are shown on the left side of Fig. 10b's CP. The values are between (18,6ho, and 120), with 60 being the mean.

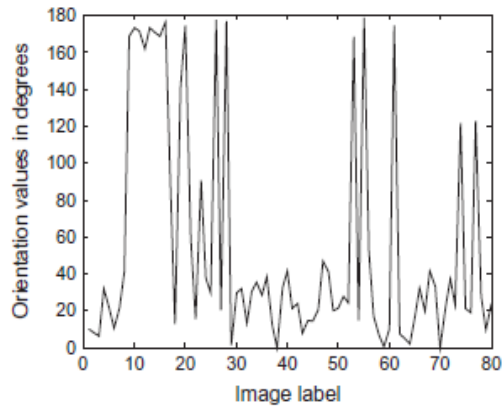
Orientation values are shown in Fig. 10c, where they have generally risen, with an average of roughly 80\_, below the CP. The maxima occur around zero and 180 degrees. When the CP is in an area of poor quality, these outlandish numbers begin to show up. They stand for some kind of background commotion. The average orientation values rise to about 100\_ on the right side of the CP, as seen in Fig. 10d. Because a loop may be either left- or right-handed, there's a wide variety of possible orientation values. That's why you may have the loop's parallel sides point left or right. The demonstration of Property 3 is supported by these orientation values. If you imagine a horizontal line that passes across the points of intersection of the ridges

#### 4. Proposed core point detection

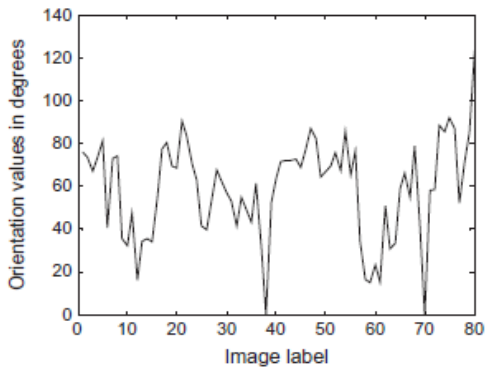
The suggested mask is introduced, and the whole CP detection technique is detailed. Using a range between 0 and 1, the given core detection mask The DL on the ridge orientation map corresponds to the highest point on the innermost ridge.

##### **The construction of the proposed mask**

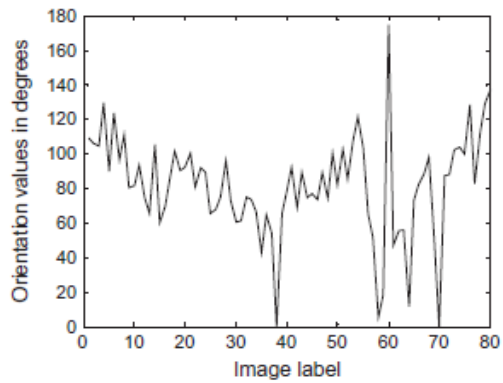
This investigation and the study performed on the orientation field of a zero-pole model [15] are both compatible with the CP. Figure 9 displays the values of block orientations relative to the CP. The value of the upper-middle block is close to zero, whereas that of the upper-right block is close to one hundred eighty. Similar to the region of the loop when the sides are parallel, the values in the three bottom blocks are close together. In the blocks around the CP, the orientation values rise from close to 0 to close to 180 in a circular manner. Each and every CP manually retrieved from pictures 10 in the training set conforms to this orientation pattern. Above the CP, the orientation values shown in Fig. 10a are either high (160\_ 6 ho 180\_) or low (0\_ 6 ho 50\_). The orientation values are shown on the left side of Fig. 10b's CP. The values are between (18,6ho, and 120), with 60 being the mean. Orientation values are shown in Fig. 10c, where they have generally risen, with an average of roughly 80\_, below the CP. The maxima occur around zero and 180 degrees. When the CP is in an area of poor quality, these outlandish numbers begin to show up. They stand for some kind of background commotion. The average orientation values rise to about 100\_ on the right side of the CP, as seen in Fig. 10d. Because a loop may be either left- or right-handed, there's a wide variety of possible orientation values. That's why you may have the loop's parallel sides point left or right. The demonstration of Property 3 is supported by these orientation values. If you imagine a horizontal line that passes across the points of intersection of the ridges, you'll arrive at the DL. As a result, the DL concludes at the highest point of the innermost circle, the upper CP.



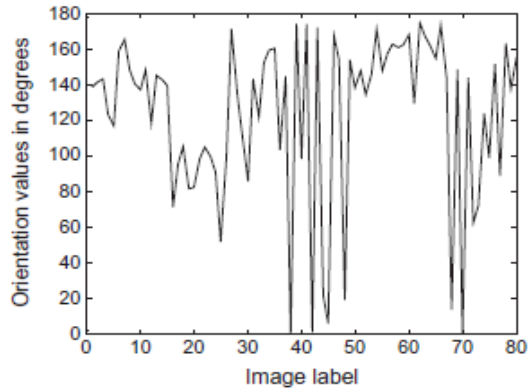
(a)



(b)

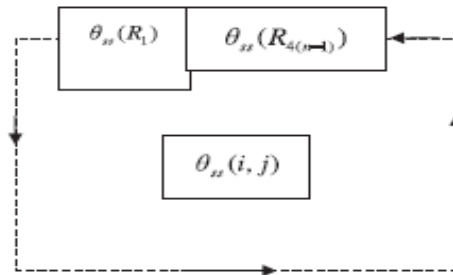


(c)



(d)

Figure 10 shows how the values for orientation rotate around a central point for a sample of blocks. Blocks a) above, b) to the left, c) below, and d) to the right.



(a)

R3	R2	R1	R16	R15
R4				R14
R5		(i, j)		R13
R6				R12
R7	R8	R9	R10	R11

(b)



You can see the suggested mask set construction in Figure 11. (a) The overall layout of the n-by-n orientation map, and (b) the blocks in the immediate vicinity that were subjected to the mask test.

$$R_k : C_k = \begin{cases} 1 & \text{if } L_k \leq \theta(R_k) < H_k \\ 0 & \text{otherwise} \end{cases} \quad (12)$$

Where k is the mask set index, C<sub>k</sub> is the conditional operation output, L<sub>k</sub> is the minimum acceptable orientation value for block R<sub>k</sub>, and H<sub>k</sub> is the value, below which value for the block's orientation is acceptable. According to this formula, we can determine how many blocks fall inside the acceptable parameters:

$$A(i, j) = \sum_{k=1}^{4(n-1)} C_k \quad (13)$$

Where the block's conditional mask answer, A (i, j), is added together. (i, j). A major CP block is identified if the calculation yields (n • n) or ((n • n) \_1). Step 3 is reached when at least one main CP block has been identified. If the CP is not present, as in the arch type, then go to step 4. If just one CP block is found, its coordinates (i<sub>CP</sub>, j<sub>CP</sub>) are converted to the CP position in the (x<sub>CP</sub>, y<sub>CP</sub>) pixel in the following way:

$$\begin{aligned} x_{cp} &= i_{cp} \times W \\ y_{cp} &= j_{cp} \times W \end{aligned} \quad (14)$$

If there is more than one CP block, the one with the lowest consistency value, as shown in equation (11), is selected as the CP.

$$CP_{block} = (i_{cp}, j_{cp}) = \underset{ij}{\operatorname{argmin}} \{ \operatorname{cons}(i, j) : A(i, j) = a \} \quad (15)$$

Thus, in step 4, the DL is identified using the edge detection technique described in [12], and the CP is defined as the DL-adjacent point. Using the minimal consistency value by multiplying (15) and then (14) to determine where the CP really is. Detecting essential points: Method 4.2 the method for detecting CP is shown in Fig. 12. Each pixel in the fingerprint scan is w pixels by w pixels. Next, the

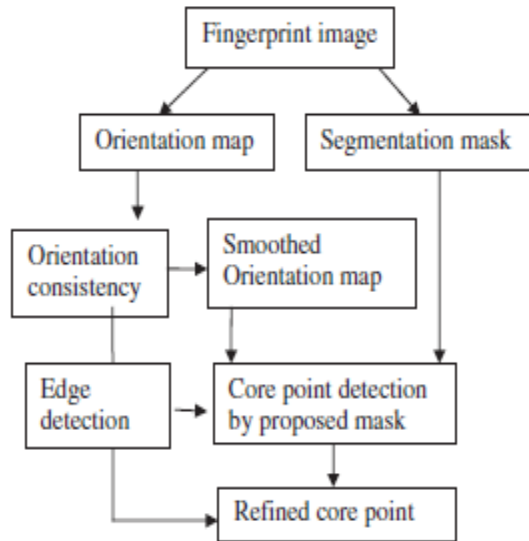


*Figure 12: A block schematic of the suggested mask for detecting the core point.*

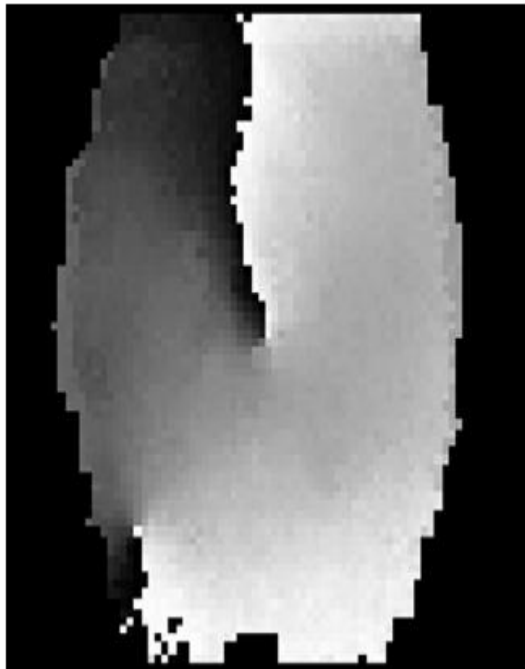


*Figure 13 shows the orientation map after the segmentation mask was applied.*



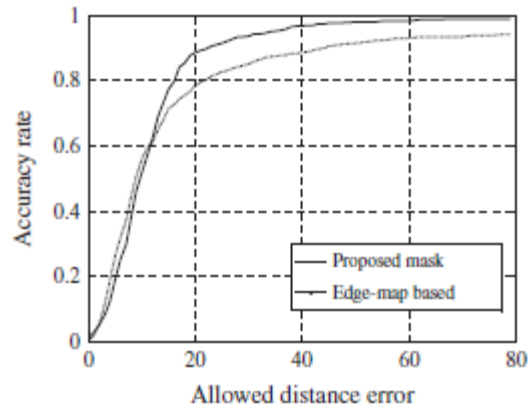
Each block undergoes a segmentation process. A segmentation scheme is established. In terms of how far the fingerprint regions (foreground) are from the rest of the picture. To avoid erroneous CP detection, it is applied to the compass orientation map. Each block's mean is computed as a percentage of the global mean of the picture, and each block's variance is computed as a percentage of the difference between the highest and lowest variance values of the whole image. If the block's relative mean is below an upper limit (mth) and its relative variance is below a lower limit (lth), then the block is divided into sub blocks. (vth). Dilation and erosion, two morphological procedures, are used to fill the gaps in the foreground and separate the points in the background, respectively [19]. Dimensions of the structural elements are (str). Figure 13 displays the segmented smoothed orientation map. A minimum-error method is used to determine the parameters. Each block is solved using the gradient-based approach [8] with an average window size of  $w \cdot w$ , as shown in equations ((6)-(10). The orientation map is smoothed using an adaptive smoothing approach [9] based on the equation (11). The suggested CP mask set scans the segmented orientation map, using blocks of size  $n \cdot n$ . Then, we use the procedure described in [9] to determine the CP orientation.

## 5. Experimental results and discussion

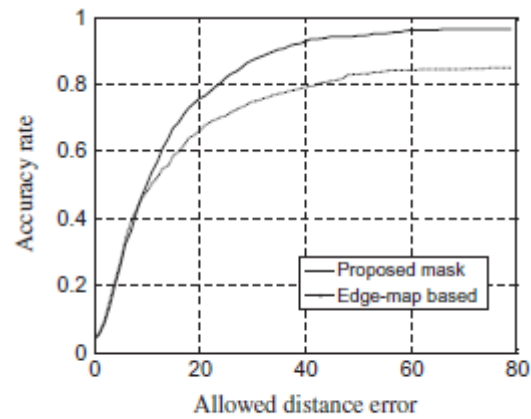
The effectiveness of the CP detection strategies is evaluated using the FVC2002 DB1 and DB2 databases [25, 26] and the FVC2004 DB1 set (B). Both FVC2002 DB1 and FVC2004 DB1 fingerprints use an optical sensor with a resolution of 500 pixels by 500 pixels. For FVC2002, the picture size is 500 by 500 pixels, while for FVC2004, it's 640 by 480. A capacitive sensor with the same resolution as DB2 is used to capture the picture. The dimensions of the photos are 256364. There are two groups in the data banks. There are eight impressions in each set. Each of the eight impressions is made from dry, moist, and normal skin. The suggested mask parameters are determined by the threshold values of the segmentation technique and the orientation values around the CP, both of which are measured using the learning set FVC2002 DB1 set (B). The DB1set (A) and DB2set (A) from FVC2002, as well as the DB1set (A) from FVC2004, are used for the tests. (B).  $w = 5$  pixel blocks make up the fingerprint picture [9]. The ridge width is exceeded by this measurement by a little margin. In order to find good parameter settings for segmentation. Each database has its own unique values for the segmentation method parameters (mth, vth, and str). Sixteen photos from the FVC2002 batch (B) are manually segmented. The settings of the segmentation algorithm are adjusted such that the discrepancy between manually segmented blocks and algorithm-segmented blocks is as little as possible.  $mth = 5$ ,  $vth = 0.1$ , and  $str = 3$  pixels are the values to use for these parameters. The CP pattern sizes tried are 3x3 and 5x5. With a mask size of 33 pixels ( $n = 3$ ), noise is easily detected. When compared to an edge-map based approach, its accuracy suffers. According to Figure 11, the suggested mask size is  $5 \cdot 5$  ( $n = 5$ ) pixels.

The orientation values limit of each block  $\theta_L(R_k) = [L_k, H_k]$ , are given in degrees as follows:  $\theta_L(R1) = \{[0, 50] \cup [120, 180]\}$ ,  
 $\theta_L(R2) = [0, 80]$ ,  $\theta_L(R3) = [15, 90]$ ,  $\theta_L(R4) = [15, 95]$ ,  
 $\theta_L(R5) = [15, 100]$ ,  $\theta_L(R6) = [20, 120]$ ,  $\theta_L(R7) = [20, 115]$ ,  
 $\theta_L(R8) = [25, 125]$ ,  $\theta_L(R9) = [40, 140]$ ,  $\theta_L(R10) = [40, 150]$ ,  
 $\theta_L(R11) = [40, 160]$ ,  $\theta_L(R12) = [40, 165]$ ,  $\theta_L(R13) = [60, 175]$ ,  
 $\theta_L(R14) = [100, 180]$ ,  $\theta_L(R15) = [122, 180]$  and  $\theta_L(R16) = \{[120, 180] \cup [0, 40]\}$ .

These metrics are used to evaluate the efficacy of various CP detection techniques:   
 \_ Core detection rate: Calculated by dividing the total number of CPs by CPs found by the algorithm to the total number of CPs found by human eyes.   
 Calculated by dividing the total number of false CPs identified by the algorithm by the total number of CPs detected by hand, we get the false alarm rate. The fake points are located in remote areas relative to the CP. The percentage of fingerprints for which the algorithm properly identified at least one characteristic pattern (CP) is known as the "correct detection rate" for fingerprints.



(a)



(b)

Experimental findings from the FVC2002 DB1B and DB2B databases are shown in Figure 14.

Table 1 The average accuracy of the core point detection algorithms (in percentage).

		Edge-map	Proposed mask	Proposed mask with DL detection
Core detection rate	FVC2002 DB1 A	89.99	97.56	96.66
	FVC2002 DB2 A	78.46	91.44	91.06
	FVC2004 B	82.5	81.25	87.5
False alarm rate	FVC2002 DB1 A	10.01	2.44	3.34
	FVC2002 DB2 A	21.34	3.56	3.94
	FVC2004 B	17.5	18.75	12.5
Fingerprint correct detection rate	FVC2002 DB1 A	84.21	97.56	96.66
	FVC2002 DB2 A	70.28	91.44	91.06
	FVC2004 B	81.25	81.25	87.5



Table 2 The average execution time of the core point detection (in ms).

	Edge map (DB1)	Proposed mask (DB1)	Proposed mask with DL detection
FVC2002 DB1 A	67.5	11.1	33.9
FVC2002 DB2 A	97.3	15.2	43.8
FVC2004DB1 B	9.6	1.5	8.1

discovered evidence. We compare the effectiveness of the suggested CP detection technique to that of the quick edge-map based method to prove the efficacy of our approach. This falls under the same heading as the suggested approach. For FVC2002's DB1 and DB2 set databases, a comparison of the suggested mask's performance with and without the DL detection is shown in Fig. 14. As the distance error margin is stretched out, accuracy improves until it reaches a plateau at around 40 pixels. When compared to the edge-map based technique, the suggested mask provides superior accuracy. With DL detection included, Table 1 also displays a comparison of performance. Since there are more arch type fingerprints in the FVC2004 database, the suggested technique that incorporates DL detection works better. For distance errors more than 10 pixels, the mask increases the rate at which the core is detected while decreasing the false alarm rate. Less than 40 pixels in length accounts for the detection lag. The results of the experiments show that the proposed method decreases the false alarm rate by 66.63% in FVC2002 DB1 (A), 58.5% in FVC2002 DB2 (A), and 28.57% in FVC2004 DB1 (B) compared to the edge-map based method, and increase the correct CP detection rate per fingerprint by 14.78% in FVC2002 DB1 (A) and 29.57% in FVC2002 DB2 (A) respectively. (B). Table 2 also displays the average execution time of the CP detection algorithms per fingerprint. It is cut by a factor of 1.19 in FVC2004 DB1 (A), 2.27 in FVC2002 DB2 (A), and 1.19 in FVC2002 DB1 (A) while using the suggested strategy. (B). Figure 15 displays the precision of the CP orientation using the procedure described in [9]. Figure 16 depicts a detected CP on the orientation map. MATLAB is used to develop the strategies, and an Intel(R) Core(TM) i3 processor running at 2.27 GHz is used to run the code.

The suggested technique is less affected by background noise. In addition,

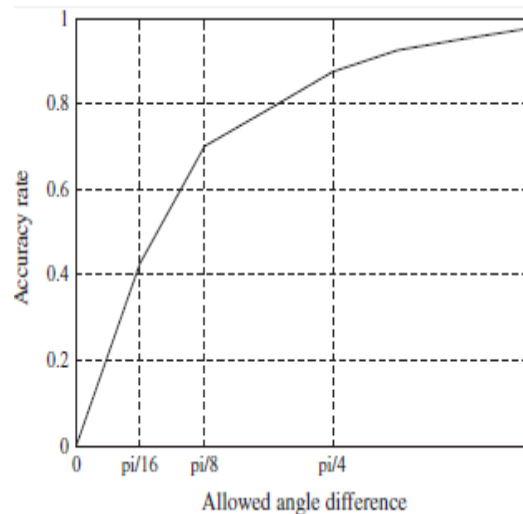


Figure 15: FVC2004 DB1 Core Point Orientation Test Results (B).

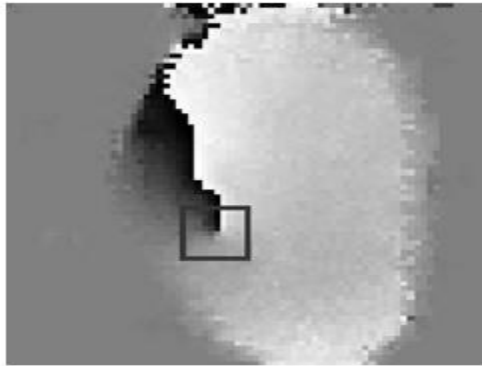


Illustration 16: A CP discovered using the suggested mask superimposed on an orientation map. On the CP location orientation map. On top of that, the layout mask's matching-condition foundation rather than



17th Figure CP identified in an up-thrust fingerprint arch. Reduces runtime by avoiding operations on orientation data. The digital realm would benefit more from this. Implementation in hardware. When compared to an edgemap-based approach, core identification using the mask is more effective even when no segmentation has been performed. However, there is a higher risk of false positives. As can be shown in Fig. 17, the suggested approach can identify the CP for both tented and up thrust arch types. When DL detection is included to the mask, performance improves while running time decreases. Any CPs that is on the outside of the fingerprint's visible area is disregarded as nonexistent. In this scenario, it is presumed that the standard method of alignment will be used. Out of a total of 800 photographs, 779 CPs were manually recovered from DB1A in FVC2002 and 754 CPs were extracted from DB2A in FVC2002. In FVC2004, DB1B only had 80 images. The primary source of mistakes is the fingerprint pictures' distortion, which leads to a faulty orientation map.

## 6. Conclusion

The proven attribute is used to confirm the solitary region's placement at the end of the broken line on the orientation map. Analysis of the axis rotation around the center. In a planned mask for detecting central points has been created. It is distinguished by immediately scanning the fingerprint image's ridge orientation map. As a result, the mask suites for the real-time applications lower execution time by an average of 1.8 times. For the hardware implementation to succeed, the mask design relies on a straightforward computational method. Due to an average

Page | 919



17.35% improvement in the proper core point recognition rate per fingerprint across all evaluated datasets (which consist of pictures captured by a variety of sensors and scales), this method is more robust in the face of background noise. In addition, the false alarm rate is decreased by 51.23 percent on average when compared to a fast edge-map based technique.

## References

- [1] Arjona R, Baturone I, A digital circuit for extracting singular points from fingerprint images. In: Eighteenth IEEE international conference on electronics, circuits and systems (ICECS), Lebanon; 2011. p. 627–30.
- [2] Neji N, Boudabous A, Hahrrat W, Masmoudi N. Architecture and FPGA implementation of the CORDIC algorithm for the fingerprint recognition systems. In: Eighth international multiconference on systems, signals and devices (SSD), Tunisia; 2011. p. 1–5.
- [3] Su XH, Yin LQ, Gao L, Zhang ZX. The design of fingerprint identification system based on TMS320VC5402. *Adv Mater Res J* 2012;542–543:1339–42.
- [4] Bazen AM, Gerez SH. Systematic methods for the computation of the directional fields and singular points of fingerprints. *IEEE Trans Pattern Anal Mach Int* 2002;24(7):905–19.
- [5] Park CH, Lee JJ, Smith MJT, Park KH. Singular point detection by shape analysis of directional fields in fingerprints. *Pattern Recogn* 2006;39(5):839–55.
- [6] Chaglong J, Hakil K. Pixel-level SP detection from multi-scale gaussian filtered orientation field. *Pattern Recogn* 2010;43(11):3879–90.
- [7] Chan KC, Moon YS, Cheng PS. Fast fingerprint verification using subregions of fingerprint images. *IEEE Trans Circ Syst Vid Technol* 2004;14(1):95–101.
- [8] Maltoni D, Maio D, Jain AK, Prabhakar S. *Handbook of fingerprint recognition*. 2nd ed. Springer; 2009, chapter 3.
- [9] Liu M, Jiang X, Kot AC. Fingerprint reference point detection. *EURASIP J Appl Signal Process* 2002;4:498–509.
- [10] Dass SC. Markov random field models for directional field and singularity extraction in fingerprint images. *IEEE Trans Image Process* 2004;13(10):1358–67.